Title

Thermodynamic and Kinetic Parameters for Calcite Nucleation on Peptoid and Model Scaffolds: A Step toward Nacre Mimicry

Journal

Crystal Growth & Design, 20(6)

ISSN

1528-7483

Authors

Nielsen, Anne R

Jelavić, Stanislav

Murray, Daniel

et al.

Publication Date

2020-06-03

DOI

10.1021/acs.cgd.0c00029

Peer reviewed

CRYSTAL GROWTH & DESIGN

pubs.acs.org/crystal

Article

Thermodynamic and Kinetic Parameters for Calcite Nucleation on Peptoid and Model Scaffolds: A Step toward Nacre Mimicry

Anne R. Nielsen, Stanislav Jelavić, Daniel Murray, Behzad Rad, Martin P. Andersson, Marcel Ceccato, Andrew C. Mitchell, Susan L. S. Stipp, Ronald N. Zuckermann, and Karina K. Sand*

Cite This: *Cryst. Growth Des.* 2020, 20, 3762−3771

Read Online

ACCESS | Metrics & More | Article Recommendations | Supporting Information

ABSTRACT: The production of novel composite materials, assembled using biomimetic polymers known as peptoids (N-substituted glycines) to nucleate $CaCO_3$, can open new pathways for advanced material design. However, a better understanding of the heterogeneous $CaCO_3$ nucleation process is a necessary first step. We determined the thermodynamic and kinetic parameters for calcite nucleation on self-assembled monolayers (SAMs) of nanosheet-forming peptoid polymers and simpler, alkanethiol analogues. We used nucleation rate studies to determine the net interfacial free energy (γ_{net}) for the peptoid−calcite interface and for SAMs terminated with carboxyl headgroups, amine headgroups, or a mix of the two. We compared the results with γ_{net} determined from dynamic force spectroscopy (DFS) and from density functional theory (DFT), using COSMO-RS simulations. Calcite nucleation has a lower thermodynamic barrier on the peptoid surface than on carboxyl and amine SAMs. From the relationship between nucleation rate (J_0) and saturation state, we found that under low-saturation conditions, i.e. <3.3 (pH 9.0), nucleation on the peptoid substrate was faster than that on all of the model surfaces, indicating a thermodynamic drive toward heterogeneous nucleation. When they are taken together, our results indicate that nanosheet-forming peptoid monolayers can serve as an organic template for $CaCO_3$ polymorph growth.

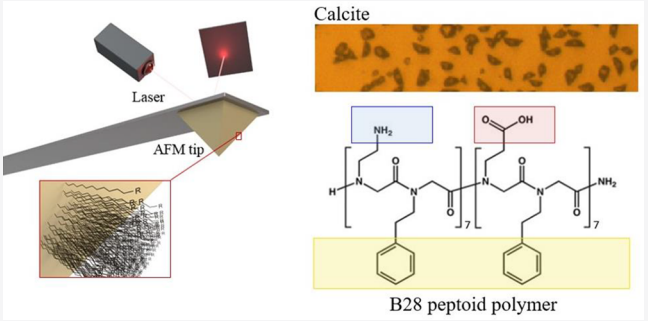

1. INTRODUCTION

Understanding how biopolymers influence the nucleation and growth of a mineral phase during biomineralization processes still represents a challenge.[1,2] Several biomineralized materials are composites where the organic material is hierarchically associated with an inorganic phase. These materials can have mechanical properties that are superior to those of the individual constituents.[3] One of the more thoroughly characterized biomaterials is the inner shell found in many mollusc species, nacre. Nacre has a layered structure with 95 vol % inorganic layers alternating with 5 vol % organic material, organized in a structure that resembles bricks and mortar at the micrometer scale. Despite the small quantity of organic material, this arrangement increases material toughness by as much as 40 times relative to the pure mineral phase.[3,4] The superior material properties of nacre have inspired nacre mimicry using a variety of components and strategies.[5−9] One proposed strategy is to mineralize 2D peptoid nanosheets with $CaCO_3$.[10] Peptoid nanosheets appear to be a promising scaffold for nacre mimicry because of their thin 2D biopolymeric structure and because their associated functional groups hold the potential to control mineral nucleation and growth. In addition, their potential for being mineralized while in suspension makes the material fabrication scalable.

Peptoids are synthetic N-substituted glycine polymers, which can be synthesized with sequence-specific control.[11,12] Some peptoids, designed with specific sequences including both hydrophilic and hydrophobic constituents, can fold to form supramolecular bilayer nanosheets.[13−17] In a previous study, Jun et al.[10] reported growing thin films of amorphous calcium carbonate (ACC) on peptoid nanosheets using the block-28 peptoid, B28.[13,14] The B28 peptoid is 28 residues in length and has both a carboxyl block (*N*-(2-carboxyethyl)-glycine) and an amine block (*N*-(2-aminoethyl)glycine); between each of the hydrophilic units is a hydrophobic unit (*N*-(2-phenylethyl)glycine) (Figure 1). The B28 nanosheets are stable in aqueous solution in the pH range that overlaps with calcium carbonate precipitation.[16] Chen et al.[18] showed that peptoid polymers containing a balance of both hydrophilic and hydrophobic groups can accelerate calcite growth, whereas polymers containing only hydrophilic groups repressed growth.

Received: January 9, 2020
Revised: April 22, 2020
Published: April 24, 2020

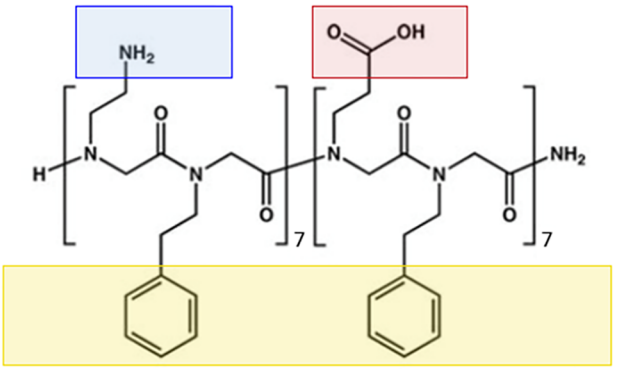

Figure 1. B28 peptoid: the hydrophilic terminations are arranged in a block of primary amine (blue) and carboxyl (red). On the opposite side of a chain is a hydrophobic unit (yellow).

Jun et al.[10] mineralized immobilized B28 nanosheets with the aim of stacking them into a layered composite material. They used the diffusion method,[19] where CO_2 was diffused through a $CaCl_2$ solution containing the nanosheets and mineralized ACC in the regime of increasing supersaturation. The downside of such a nonconstant composition approach is that it is challenging to control the nucleation processes, and the results provide little insight into the driving force for mineralization. There are two pronounced pathways for organic biopolymers to induce $CaCO_3$ precipitation. The first is where charged organic functional groups bind Ca^{2+} or CO_3^{2-} and locally increase the $CaCO_3$ supersaturation around the polymer, promoting $CaCO_3$ nucleation.[20] Second, some biopolymers can decrease the thermodynamic barrier (ΔG^*) for forming a nucleus of a critical radius. ΔG^* decreases when the net interfacial free energy for the crystal−substrate−liquid interface (γ_{net}) is lower than the interfacial free energy for the crystal−liquid interface (γ_{cl}).[21,22] In such a case the mineralization can occur heterogeneously on the polymers rather than homogeneously in the bulk solution. If heterogeneous nucleation is obtained at constant supersaturation, nucleation theory can be applied and thermodynamic and kinetic parameters derived which describe the nucleation process.[23−25] The derivation of these parameters will allow better control over the nucleation events and easier upscaling of material fabrication processes.

To upscale mineralization of the nanosheets, we explored if the B28 peptoid polymers could decrease γ_{net} and hence induce $CaCO_3$ nucleation on the nanosheets. We used a strictly controlled set of solutions designed to enable nucleation of calcite (the most stable polymorph of $CaCO_3$). We subsequently obtained thermodynamic and kinetic parameters to describe the interactions between the substrates and the $CaCO_3$. To address the contribution from the two different hydrophilic functional groups in the peptoids, we expanded our experimental matrix to include three self-assembled monolayers (SAMs) with headgroups containing only (a) carboxyl and (b) amine functional groups and (c) a mix of the two, such as is found in B28. To get comprehensive insight into the nucleation of calcite on our nacre-mimicking organic scaffolds, we used three distinct techniques to address the thermodynamic and kinetic driving force for $CaCO_3$ mineralization: (A) Steady-state nucleation rate (J_0) experiments, where we measured the nucleation rate of calcite, and related it to ΔG^* and γ_{net}. (B) Dynamic force spectroscopy (DFS) was used to obtain bond parameters between the substrate and calcite to calculate the Gibbs free energy of binding (ΔG_b). Having ΔG_b, we estimated a decrease in γ_{net} during heterogeneous nucleation of $CaCO_3$ as a function of substrate composition. (C) Density functional theory (DFT, COSMO-RS) was used to calculate γ_{net} of the calcite−substrate interfaces. Thus, our approach combines evidence from studies at the bulk scale (nucleation rate), bond level (DFS), and simulations (DFT) and provides a robust characterization of the parameters that control calcite nucleation on the B28 scaffold. This study allowed us to investigate if and under what solution conditions nanosheets could be used as a scaffold for calcite nucleation and for growth of biomimetic materials, thus moving one step closer to nacre mimicry.

2. EXPERIMENTAL SECTION

2.1. Preparation of B28 Peptoid Substrates and Alkanethiol SAMs. We synthesized the B28 peptoid on an Aapptec Apex 396 robotic synthesizer using the solid-phase, submonomer method and purified the polymers by reverse-phase HPLC.[12,14,16] We dispersed lyophilized peptoids in a 2/1 % v/v mixture of dimethyl sulfoxide (DMSO) and ultradeionized water to obtain a 2 mM peptoid stock solution. We used highly oriented pyrolytic graphite (HOPG) as the substrate for functionalization because the B28 peptoids self-assemble on HOPG by adhering through their hydrophobic units. We prepared a 100 μM peptoid solution by mixing 25 μL of 2 mM peptoid stock solution in 2/1 DMSO/H_2O with 50 μL of a 100 μM aqueous solution of TRIS (tris(hydroxymethyl)aminomethane) to buffer the solutions to pH 8 and 425 μL of ultradeionized water (Milli-Q, resistivity >18.2 MΩ cm). We prepared the B28 peptoid substrate by placing a 30 μL droplet of the 100 μM peptoid solution on a freshly cleaved HOPG substrate and let it equilibrate for 1/2 h in a closed, humidity-controlled container. We flushed the B28 substrate with 15 mL of ultradeionized water to remove excess polymer. To remove as much liquid as possible, we placed the substrates on a paper tissue with the B28 peptoid functionalization facing up. We placed the B28 peptoid substrate back into the humidity-controlled container, pipetted a 20 μL droplet of ultradeionized water onto the surface, closed the container, and left the substrate to dry. The substrate was then rinsed again with 15 mL of ultradeionized water and dried using a jet of N_2, thereby removing excess material. We used an Asylum Research MFP 3D atomic force microscope (AFM) with tips from Olympus to image the formed layer.

As a control surface, we prepared a second type of substrate from SAMs of alkanes bearing the same ionic functional groups that the peptoid has. We prepared self-assembled monolayers (SAM), with terminations composed of the same functional groups as those on the nanosheet surface (e.g., carboxyl (carboxyl SAM), amine (amine SAM) and a mix of the two (1:1 SAM)). The SAMs were made using alkanethiols that allow the molecules to bind covalently to Au via the terminal thiol group, thus producing highly organized layers.[26,27] The surface chemistry of the part of the SAM that is exposed to solution is then defined by the functional group (headgroup) at the other end of the alkanethiol molecule. We prepared two alkanethiol stock solutions: (i) 11-mercaptoundecanoic acid (98% $HS(CH_2)_{10}COOH$, Sigma-Aldrich) and (ii) 11-amino-1-undecanethiol hydrochloride (99% $HS(CH_2)_{11}NH_2$, Sigma-Aldrich), each with a concentration of 2 mM, using anhydrous ethanol (≥99.8%, HPLC grade, VWR chemicals) as the solvent. To minimize adventitious carbon on the substrate surface, we produced Au substrates ourselves. We cleaned Si wafers, purchased from Ted Pella (5 × 7 mm chips), in 10 mL of anhydrous ethanol, rinsed them with 30 mL of ultradeionized water, and repeated the cleaning in anhydrous ethanol. Subsequently, we sonicated the Si wafers in 10 mL of acetone (≥99.5% analytical grade, Sigma-Aldrich) for 20 min. Using two-component epoxy (EPO TEK 377), we glued the freshly cleaned Si wafers face down on Au-coated Si wafers (PLATYPUS). The wafers we chose had no Ti or Cr adhesion layer between the Si and the Au, which meant that after

https://dx.doi.org/10.1021/acs.cgd.0c00029
Cryst. Growth Des. 2020, 20, 3762−3771

curing for 1 h at 150 °C the small Si wafers were ready to be clicked off to obtain fresh, clean Au surfaces, ready for immediate funcionalization.

The SAM functionalization methods were adapted from Nielsen et al.[28] for the carboxyl SAM and from Chuang et al.[29] for the amine and 1/1 SAMs. We initiated the SAM functionalization by placing 4 mL of the stock thiol solution on a UV/ozone-cleaned glass Petri dish (20 min, UV/Ozone ProcleanerTM, BioForce nanosciences). To improve the dispersion of the carboxyl SAMs, we added acetic acid to a final concentration of 6% to a Petri dish (≥99.8%, Sigma-Aldrich),[28] and for amine and 1/1 SAMs, we added triethylamine to a final concentration of 3% (≥99%, Sigma-Aldrich).[29] The Au substrates were clicked off and submerged into the alkanethiol solution. We left the wafers to equilibrate in the thiol solution for 24 h. The freshly made SAMs were rinsed with 3−5 mL of anhydrous ethanol, then with 3−5 mL of 1% HCl in anhydrous ethanol, and again with the anhydrous ethanol to remove the unbound molecules. The functionalized SAMs were dried with a jet of N_2 and used immediately in the experiments. To verify the composition of the SAMS, we examined a few with X-ray photoelectron spectroscopy (XPS) (Figure S1 and S2). The SAM surfaces had ∼75% coverage with bound thiols, which we determined by comparing the peak ratio in the S 2p high-resolution spectrum of S bonded to Au to S chemisorbed to Au (Figure S3). For the 1:1 SAM, we added a 90%/10% v/v mix of 11-mercaptoundecanoic acid and 11-amino-1-undecanethiol hydrochloride and obtained a substrate with an average of 50% carboxyl and 50% amine coverage, which we determined by comparing the intensities of the carboxyl peak and nitrogen peak from their high-resolution spectra.

2.2. Nucleation Rate Experiments. In previous studies, steady state nucleation rates (J_0) have been used to derive parameters for the kinetic and thermodynamic contributions to calcite nucleation.[23−25,30] J_0 was determined from the data of steady-state flow experiments, where nucleation was observed as a function of time. In these studies, the saturation index (σ) was defined by:

$$\sigma = \ln\left(\frac{a(Ca^{2+})a(CO_3^{2-})}{K_{sp}}\right) \quad (1)$$

where a represents the ion activity and K_{sp} represents the equilibrium constant for calcite formation. By a plot of the number of nuclei as a function of time, J_0 is determined from the slope of the linear fit. From nucleation theory, we know that:

$$\ln J_0 = \ln A - \frac{B}{\sigma^2} \quad (2)$$

where A represents a prefactor dependent on kinetics (diffusion or attachment and detachment of ions at the surface) and B represents a thermodynamic factor that is proportional to ΔG^* and is related to γ_{net}. By plotting $\ln J_0$ as a function of $1/\sigma^2$, B was determined from the slope of a linear fit and $\ln A$ was determined from the y intercept.

To measure the steady-state nucleation rate for calcite on the functionalized substrates in the solutions, we used a flow-through system that ensured controlled supersaturation (σ) throughout the experiment (Figure S4). We prepared solutions of $CaCl_2{\cdot}2H_2O$ (99%, Sigma-Aldrich) and $NaHCO_3$ (99%, Sigma-Aldrich) using ultra-deionized water and diluted the 100 mM solution to 7−11 mM $CaCl_2$. We verified calcium ion concentrations using flame atomic absorption spectroscopy (PerkinElmer AAnalyst 800). We calibrated a pH meter using standard buffer solutions of pH 4, 7, and 9 (Metrohm) and prepared 7−11 mM $NaHCO_3$ solutions, which we titrated to pH 9.5 ± 0.1. We used fresh $NaHCO_3$ solutions that we prepared immediately before the experiments to minimize pH change as a result of reaction with CO_2 in air. We transferred the $CaCl_2$ and $NaHCO_3$ solutions into two 60 mL polypropylene (PP) syringes and placed them in a double syringe pump (WPInstuments). The experiments were conducted at ambient temperature, 23 °C.

Prior to the experiment, we mounted the functionalized substrates in a custom-made flow cell, sealed it, and placed it under an upright optical microscope (ZEISS Axio Imager). Using poly(ether ether ketone) (PEEK) tubing, with an inner diameter of 0.5 mm, we connected the syringes with a static mixer (Analytical Scientific, 50 μL), which by its inner design mixes the two input solutions, and connected the mixer with the flow cell. The small diameter and the small volume of the mixer minimized the dead volume between the solution mixing point and the point where the supersaturated solution reached the sample. A low dead volume is important for minimizing homogeneous nucleation, which would change the conditions in the flow cell from the known σ and pH 9.0 ± 0.1 to something unknown. The experiment was started by applying a steady flow (2 mL/min for each syringe) providing a flux of 0.08 mL/(mm^2 min) over the sample. The flux was chosen to avoid diffusion-limited conditions.[23] During the experiments, we imaged the sample and counted nucleation events as a function of time. We operated the optical microscope with a 10× magnification in the objective, in bright field reflecting light mode where white light was reflected from the sample surface. We collected images in time steps of 0.25 s, and each experiment lasted 20−30 min.

We used the geochemical speciation code PHREEQC[31] with the phreeqc.dat database to calculate σ. In PHREEQC, σ is defined using $\log_{10}$ instead of ln (eq 1); thus the output from PHREEQC was multiplied by ln 10. We used a K_{sp} value for calcite of $10^{-8.48}$.[32] The calculation showed σ to be in a range between 5.25 and 5.85, which is consistent with the work of Giuffre et al.[25]

We used a field emission scanning electron microscope (Quanta 3D FEG SEM) to examine the samples after the nucleation rate studies. We placed the SAMs on a stub with double-sided carbon tape. No coating was used. We used an acceleration voltage of 5 kV, a current of 6.7 pA, and a spot size of 3.5.

2.3. Dynamic Force Spectroscopy. We used an Asylum Research MFP 3D AFM instrument and MSCT tips from Bruker for DFS measurements. We cleaned the tips and the tweezers in a UV/ozone cleaner for 20 min and functionalized the tips with SAMs in the same way as we produced the SAMs for the nucleation measurements. Iceland spar (purchased from Ward's Scientific) was cleaved along the {10.4} face, placed in the AFM liquid cell, and immediately covered with the calcite-saturated solution (pH 8.2). The time lapse between cleaving the crystal and covering it with a solution was <1 min. The tip containing a functional group was brought into contact with the calcite surface at a rate of 100 nm s^{-1} until a trigger force of 100 pN was reached. The tip remained at the surface (dwell time) for 1 s, and then it was retracted to 500 nm from the sample. We collected force curves at 7 different retracting velocities, ranging from 5 to 10000 nm s^{-1}. We collected at least 100 force curves per retracting velocity, amounting to at least 700 force curves per experiment. We made between 2 and 5 consecutive experiments in the same solution with the same crystal because Iceland spar is a mineral with natural variations in trace element concentration that could affect the results. The data from each set of experiments were combined during the data processing so that each force spectrum represented 1400−3500 individual force curves. During the experiments, we moved the tip over the surface in a random walk, with a step size of 10 nm to account for various surface heterogeneities. The experiments were conducted using a nominal cantilever spring constant. The effective spring constant (k), used for data treatment, was determined from the thermal calibration method at the end of the experiment.[33] The rupture forces (f) were corrected for the true value of the spring constant at the data processing stage. An average of all rupture forces ($\bar{f}$) per retracting velocity (v_{ret}) was determined and plotted as a function of the loading rate (r). We calculated r as a product of the nominal v_{ret} and k. Once plotted, we used a fit to the Friddle model[34] and we obtained the equilibrium rupture force under static conditions (f_{eq}) and the distance between the bound and the unbound state (x_t). These parameters were used to calculate the Gibbs free energy of binding (ΔG_b):[34]

$$\Delta G_b = k_B T \ln\frac{f_{eq} x_t}{k_R T} + f_{eq} x_t + k_B T \quad (3)$$

https://dx.doi.org/10.1021/acs.cgd.0c00029
Cryst. Growth Des. 2020, 20, 3762−3771

where k_b represents the Boltzmann constant and T the temperature in K.

2.4. COSMO-RS: Interfacial Free Energy Simulation. We carried out density functional theory (DFT) calculations using the COSMO-RS implicit solvent model[35] to calculate the interfacial tension among water, calcite, and the SAMs. We used Turbomole,[36] the BP functional,[37,38] the TZVP basis set,[39] and COSMO implicit solvent[40] with infinite dielectric constant, which is required for the subsequent COSMO-RS calculations. We used the BP-TZVP parametrization from 2016[41] for the COSMO-RS calculations and a temperature of 298 K. In the creation of the COSMO surfaces to model the surface of the SAMs, only the functional groups were included in the calculations because the aliphatic chains of the SAMs only interact with each other and not with the water or calcite. The γ value was calculated using our model for solid−liquid γ,[42] which is based on our model for predicting liquid−liquid γ.[43] In all solid−liquid γ calculations, the SAM functional groups were treated as the solid surface, using a weight factor of 0 for all other atoms in the model molecules for the COSMO-RS calculations. This way only the parts of the molecules exposed to the solution are being included in the surface energy calculations. The nucleated calcite was modeled using a small cluster, consisting of 80 atoms (16 $CaCO_3$ units in a rhombohedral arrangement). For modeling of the SAM surfaces, two molecules were used for each SAM, with a distance between them taken from the known lattice spacing of SAMs formed on gold, which is 5 Å. We optimized the geometry for a single molecule, such that the aliphatic chain was aligned with the z axis. We then copied and subsequently translated the coordinates 5 Å along the x axis. The functional group and the attached CH_2 for each molecule were allowed to relax during the calculations, to allow for direct interactions between surface groups such as hydrogen bonding. The Cartesian coordinates of the carbon atoms in the aliphatic chains not in the functional group or adjacent to it were frozen to mimic the ordered structure of the SAM not exposed to the solution. The surface models used in the calculations were (i) a carboxylic acid dimer as a model for COOH-SAM, (ii) an amine dimer as a model for NH_2-SAM, and (iii) one carboxylic acid and one amine as a model for the 1:1 SAM. This setup allowed us to take into account possible internal hydrogen bonding in the surface.[44]

3. RESULTS AND DISCUSSION

3.1. Nucleation Rate Measurements. The B28 peptoid polymers produced a relatively uniform SAM containing drying cracks on the HOPG surface (Figure 2a). The SAM thickness was ∼1.5 nm, measured by AFM (Figure 2b). The measured thickness corresponds to the height expected for a B28 peptoid monolayer organized with the hydrophobic phenyl groups adhering to the graphite surface and the hydrophilic groups exposed toward the solution.[13,14,16,45]

We nucleated $CaCO_3$ on carboxyl, amine, 1/1, and B28 SAMs and counted the number of nucleation events as a function of time using a light microscope. From the nucleation rate experiments, we obtained the steady-state nucleation rate (J_0) for the peptoid and alkanethiol substrates during exposure to a range of σ = 5.25−5.85, as illustrated in Figure 3. J_0 increases systematically with increasing σ for each of the substrates investigated. We observed a similar trend in incubation time where high driving forces for nucleation promoted a low incubation time. Optical microscopy images of the $CaCO_3$ crystals obtained at different time steps on the SAMs and B28 substrates are presented in Figures S5−S8. The morphology of the crystals resembles calcite crystals, as expected for our experimental conditions (pH 9.5 ± 0.1, σ = 5.25−5.85). Within our σ range, the carboxyl SAMs had the fastest J_0, with approximately 2400 sites min^{-1} (σ = 5.73) followed by the amine SAMs with 17 sites min^{-1} at the same σ. Surprisingly, we observed no heterogeneous nucleation on the

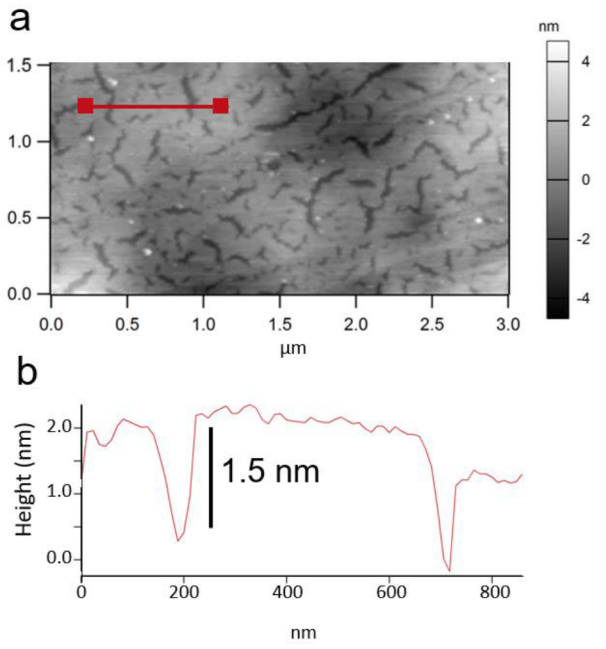

Figure 2. (a) AFM height image of B28 SAM on HOPG where light gray corresponds to higher areas, in this case the B28 SAM. Cracks in the monolayers are seen as dark gray. (b) Vertical profile along the red line in (a) shows the thickness of the B28 SAM, ∼1.5 nm.

1/1 SAMs and J_0 on the B28 peptoid substrates was only 0.8 sites min^{-1} (σ = 5.73). The B28 and the 1:1 SAM have different spatial distributions and intermolecular packings of the carboxyl and amine groups, and the difference in nucleation rates that we observe can be explained as the difference in surface charge and structure between the two substrates.[25] The block nature of B28 peptoid implies that the organization of carboxyl and amine groups is sequential, whereas for the 1:1 SAM the distribution of functional groups is less ordered. The sequential structure of B28 would display patches of different charges on its surface which would affect the diffusion of molecules around the critical nuclei and also affect the collision probability.[46] The less ordered surface distribution of the carboxyl and amine groups of 1:1 SAM would result in interactions between these differently charged groups which effectively could neutralize the surface charge. Similar observations of variations in nucleation rates between polymers that differ slightly in structure have been made by Hamm et al.[24] and Giuffre at al.[25]

To parametrize the thermodynamic and kinetic contributions to nucleation rates, we plotted ln J_0 as a function of $1/\sigma^2$ (eq 2 and Figure 4). Linear fits (eq 2) provide (Table 1) the following: (i) the slope, B, which is proportional to the thermodynamic barrier for nucleation (ΔG^*), and (ii) the intersect of the line with the y axis, ln A, which is the kinetic parameter that accounts for the rate of ion diffusion, ion desolvation, attachment, and detachment. For the range of explored σ, the B28 peptoid substrate has the lowest B but also the lowest ΔG^* in comparison with the other SAMs. The second lowest barrier is for the carboxyl SAM, and the amine SAM has the highest barrier. Possibly counterintuitively, the lowest B and thereby ΔG^* do not correlate with the highest J_0 at every σ. Equation 2 implies that the lower the B, the lower the J_0. However, this is only the case at the supersaturations at which the thermodynamic contribution (B) to the nucleation

https://dx.doi.org/10.1021/acs.cgd.0c00029
Cryst. Growth Des. 2020, 20, 3762−3771

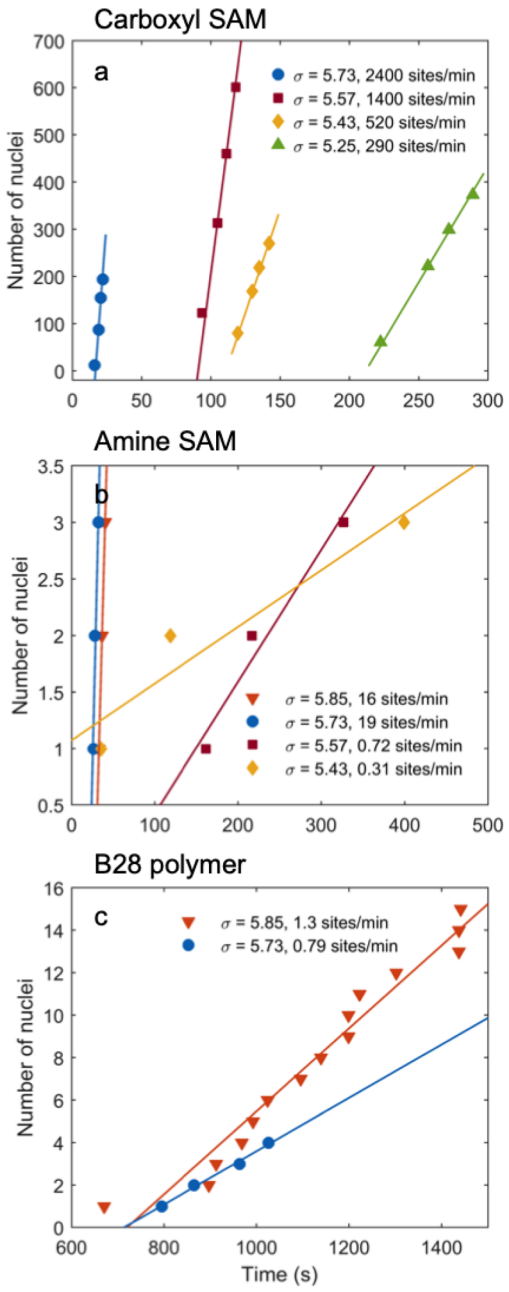

Figure 3. Number of heterogeneous nucleation events as a function of time at various σ: (a) carboxyl SAM, (b) amine SAM, and (c) B28 peptoid substrates. Colored lines are linear fits to the data.

rate overcomes the kinetic contribution (A). That is, when J_0 values are compared at two different substrates, there is a σ value below which the nucleation kinetics at one substrate becomes so slow that, even though the nucleation barrier is lower than at another substrate, the nucleation rate becomes slower. This is consistent with the classical nucleation theory[23,47] and observations from Giuffre et al.[25] At the range of σ where nucleation rate experiments were feasible, the relatively low ln A value for B28 peptoid substrates resulted in a J_0 value that was significantly lower than those for the carboxyl and amine SAMs. However, by extrapolation of the fits toward low σ to after the intersect between the fit of B28 and the fits to the SAM data, the nucleation rate on B28 peptoid is higher than the nucleation rate on both alkanethiol

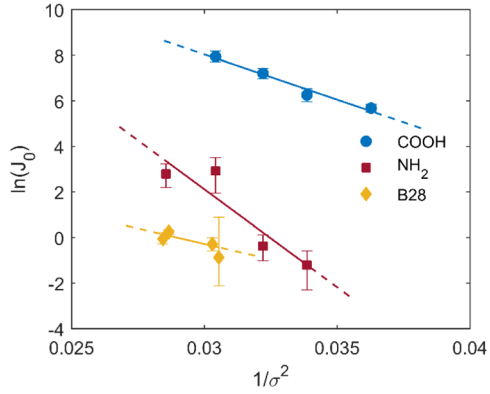

Figure 4. Plot of ln J_0 as a function of $1/\sigma^2$ (eq 2). The slope of the fit, B, is proportional to the thermodynamic barrier for nucleation, ΔG^*, and the intercept of the fit with the y axis defines the kinetic parameter ln A. The uncertainties are given by the standard error of J_0, which is determined from the linear fits in Figure 2.

Table 1. Extracted Values for B and ln A from Nucleation Rate Experiments

surface	B	ln A	J_0[b] (σ = 5.73) (site/min)
carboxyl SAM	397 ± 65[a]	20 ± 2	2400
Amine SAM	859 ± 334	28 ± 11	17
B28 peptoid	267 ± 125	8 ± 4	0.79

[a]The uncertainties are expressed as the standard error of the linear polynomial fits. [b]Obtained from Figure 2.

SAMs. This means that at low driving forces for nucleation when σ is below 3.3 (i.e., $\sigma^{-2} > 0.09$), which is where the B28 fit and the carboxyl SAM fit intersect, nucleation changes from highly saturated conditions with dominant kinetic influence to less saturated conditions, where thermodynamics dominates the J_0 value. This indicates that the mineralization of B28 nanosheets is likely favored in comparison to other surfaces when $\sigma \leq 3.3$ and provides a key insight for using nanosheets as scaffolds for biomimetic materials.

Giuffre et al.[25] showed a linear correlation between surface charge density of the substrate and B derived from nucleation rate studies, where high B correlates with high negative surface charge. Under our experimental conditions (pH 9.0), the B28 peptoid substrates are overall negatively charged because of the prevalence of deprotonated terminal groups.[48] For calcite nucleation on B28 peptoid substrates, B = 267 ± 125 is consistent with a slightly negative surface charge, as expected for B28. A B value of 390 ± 11 for calcite nucleation on carboxyl SAM was previously reported[24] for C_{16}-COOH SAMs at pH 10. This is consistent with our results. For the amine SAM, B = 859 ± 334 is approximately q times higher than for the carboxyl SAM, indicating that amine SAMs have a higher ΔG^* value than carboxyl SAMs, suggesting that, thermodynamically, nucleation on carboxyl SAMs is more favorable than on amine SAMs.

The morphologies of the particles nucleated at the carboxyl, amine, and B28 SAMs were prevalently prismatic (Figure 5a), rhombohedral (Figure 5b), or a mixture of both (Figure 5c). Prismatic and rhombohedral forms are typical for a trigonal system in which calcite crystallizes, and considering the system is designed to precipitate calcite,[23] we interpreted these crystals to be calcite. The face of a calcite crystal nucleated on a substrate is the least energetically demanding face: i.e., the face

https://dx.doi.org/10.1021/acs.cgd.0c00029
Cryst. Growth Des. 2020, 20, 3762−3771

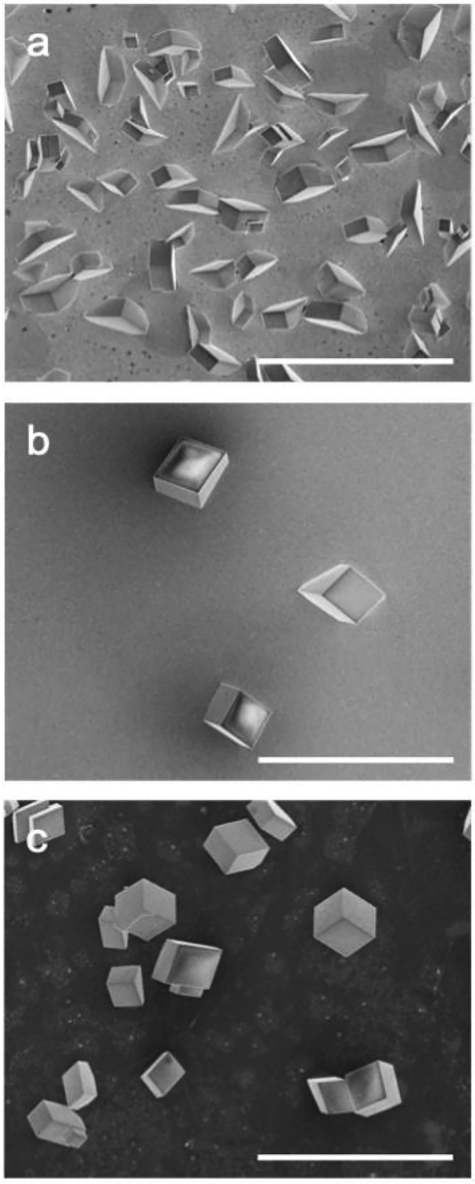

Figure 5. SEM images of heterogeneously grown calcite on (a) carboxyl SAM, (b) amine SAM, and (c) B28 peptoid substrate. Scale bars are 50 μm.

presenting the lowest γ_{net}. From SEM images, we interpreted the orientation of the calcite on all three substrates. The carboxyl SAM favored calcite with prismatic and tabular crystal habit, characteristic for nucleation on the {01.2}, {01.3}, and {01.5} faces (Figure 5a).[23,49,50] Calcite crystals on the amine SAM were rhombohedral, indicating nucleation on the {10.3} face (Figure 5b).[50] On the B28 peptoid substrates, the crystal form and orientation varied, suggesting that they formed on a surface where functional group ordering was heterogeneous (Figure 5c).

3.2. Gibbs Free Energy of Binding (ΔG_b) between Calcite and Organic Surfaces. To obtain binding parameters between calcite and the carboxyl, amine and 1/1 SAMs (Table S2) and calculated their ΔG_b values (eq 3), we used DFS (DFS was not possible on the B28 polymer because of the difficulty in immobilizing the polymer on the tip). The ΔG_b value between a polymer and a mineral surface is proportional to γ_{net}:[24] i.e., the stronger the binding between the mineral and the polymer, the lower the γ_{net}, and as a result, the more favorable the formation of a mineral nucleus on the polymer. ΔG_b is highest for the calcite−carboxyl SAM interface (5.0 ± 0.7 kT), followed by the amine SAM−calcite (3.6 ± 0.6 kT) and calcite−1:1 SAM interfaces (2.3 ± 0.8 kT) (Figure 6 and Table S2). This suggests that calcite nucleation

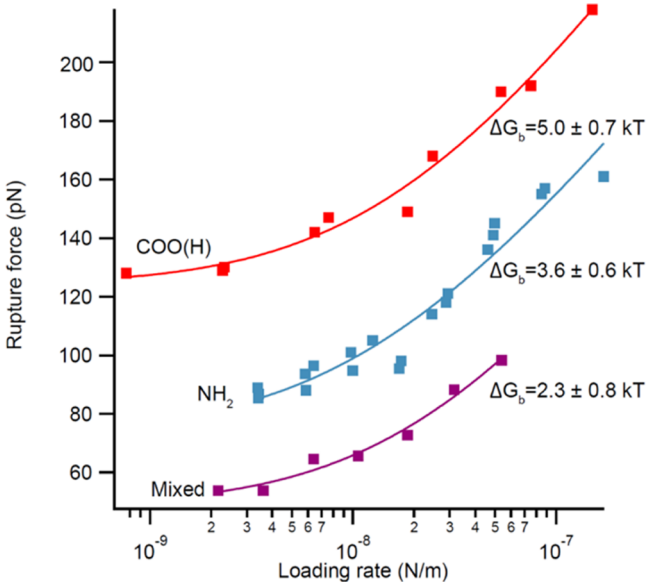

Figure 6. Rupture forces as a function of loading rate determined from DFS studies of calcite−carboxyl SAM (red), calcite−amine SAM (blue), and calcite−1:1 SAM (purple) and their ΔG_b values. The uncertainty is presented as a standard deviation propagated from standard deviations for the fitted binding parameters (Table S2).

on a carboxyl SAM is more favorable than on an amine SAM and least favorable on a 1:1 SAM, which is consistent with nucleation experiments (Figures 3 and 4, Table 1, and Figures S5−S8). For comparison, our ΔG_b value for the calcite−carboxyl SAM is ∼2.5 times lower than that reported by Hamm et al.[24] We conducted our experiments at pH 8.2, whereas Hamm et al. used pH 10.55. The point of zero charge of calcite is 8 < pH < 9.5,[51] and hence the pH used by Hamm et al. caused a larger electrostatic contribution and increased ΔG_b.

3.3. Thermodynamic Driving Force of Heterogeneous Nucleation: Obtaining γ_{net}. In general, the lower the γ_{net} value for a mineral−polymer interface, the easier the formation of nuclei on the polymer. However, only when $\gamma_{net} < \gamma_{cl}$ is heterogeneous nucleation more favorable than homogeneous nucleation. Söhnel et al.[52,53] estimated that γ_{cl} for calcite in water is 103 mJ/m^2, implying that if heterogeneous nucleation is to occur, γ_{net} must be <103 mJ/m^2.

3.3.1. Nucleation Rate Experiments: Bulk Level Approach. From the nucleation data (Figure 4 and Table 1), we calculated γ_{net}:[24]

$$\gamma_{net} = \sqrt{\frac{Bk_b^3T^3}{F\omega^2}} \quad (4)$$

where ω represents the molecular volume of calcite, which was estimated to be 6.13×10^{-29} m^3 and F represents the crystallite shape factor, set to 16 for nucleation on the {10.4} face.[24] Calcite nucleation on different faces modifies F, but this does

https://dx.doi.org/10.1021/acs.cgd.0c00029
Cryst. Growth Des. 2020, 20, 3762−3771

not change γ_{net} significantly because of the power relationship between the two. Hu et al.[23] evaluated the variation in γ_{net} to be no more than 10%. γ_{net} calculated from the nucleation rate experiments follows the trend:

$$\text{B28 (68 mJ/m}^2\text{)} < \text{COO(H) (77 mJ/m}^2\text{)} < \text{NH}_2\text{ (100 mJ/m}^2\text{)}$$

During the nucleation rate experiments, we did not observe nucleation on the 1:1 SAM; therefore, γ_{net} for this system could not be determined. γ_{cl} for calcite (103 mJ/m^2) exceeds the values of γ_{net} determined from the nucleation rate studies for the B28, the carboxyl, and amine substrates, highlighting that nucleation on the applied substrates is thermodynamically favored under the applied conditions.

3.3.2. Dynamic Force Spectroscopy: Molecular Level Approach. We extracted γ_{net} from the DFS measurements using:[24]

$$\gamma_{net} = -\left(\frac{h}{a}\right)\Delta G_b + (1 + h)\gamma_{cl} \quad (5)$$

where h represents the nucleus shape factor (the crystal−substrate interaction area divided by the surface area of the crystal exposed to solution) and a represents the area of interaction per alkanethiol polymer. Hu et al.[23] evaluated the variation of h as a result of growth on different calcite faces to be no more than 10%. We adopted the shape factor of 0.333 to represent the {10.4} calcite surface and 0.525 to represent the {01.2} calcite surface as previously assigned.[23,24,54] The value of a depends on the SAM organization on the tip; therefore, we calculated γ_{net} using a range of $0.2 \le a \le 0.6$ nm^2, where the lowest value represents a well-organized SAM[55] and the highest value represents a poorly organized SAM. The resulting γ_{net} values extracted from the DFS experiments follow a trend similar to the nucleation experiments:

$$\text{COO(H)SAM (103} \pm 3 - 137 \pm 1\text{ mJ/m}^2\text{)} < \text{NH}_2\text{SAM (111} \pm 1 - 142 \pm 1\text{ mJ/m}^2\text{)} < \text{1/1SAM(120} \pm 1 - 147 \pm 1\text{ mJ/m}^2\text{)}$$

where the minimum and maximum values in the range arise from different combinations of a and h (Tables S3 and S4). The uncertainty represents standard deviation propagated from the uncertainty on the ΔG_b values (Table S2). As observed for γ_{net} from the nucleation rate measurements, γ_{net} for carboxyl−calcite is lower than for amine−calcite. The γ_{net} for 1:1 SAM−calcite is the highest, indicating that heterogeneous nucleation on 1:1 SAM is not favorable. This result is consistent with the lack of nuclei observed on 1:1 SAM during the nucleation rate measurements and provides an explanation based on behavior at the molecular level.

3.3.3. COSMO-RS Modeling: Computational Approach. We used computational modeling, COSMO-RS, to calculate γ_{sl} and γ_{cs} (Table S5) from first principles. γ_{net} was then determined from:

$$\gamma_{net} = \gamma_{cl} - h(\gamma_{sl} - \gamma_{cs}) \quad (6)$$

where γ_{sl} represents the substrate−liquid free interfacial energy and γ_{cs} represents the crystal−substrate free interfacial energy. h was again assumed to be between 0.3 and 0.5. To account for the influence of SAM charge on γ_{sl} and γ_{cs}, the calculation was carried out for surfaces of dimers varying in their degree of protonation. This means γ_{net} for the carboxyl surface was determined for COOH−COOH (net charge 0), COOH−COO^- (net charge −1) and COO^-−COO^- (net charge −2). Similarly, for amine the calculations were conducted for NH_2−NH_2 (net charge 0) and NH_2−NH_3^+ (net charge +1), whereas for the 1/1 layer, only COO^-−NH_3^+ (net charge 0) was considered. The results of the COSMO calculations are shown in Figure 6 and in Table S5. We did not measure the acidity constants (pK_a) for our SAMs, but the theoretical pK_a for the carboxylic group is ∼4.5 and for the amine group is ∼10.[56] The pK_a values of the carboxylic and amine groups are different in bulk solution in comparison to a closely packed SAM, but are generally close to the theoretical values. Regardless of the apparent value of pK_a, the carboxyl SAM is negatively charged and the amine SAM is not charged at pH 9 in pure water. However, in solutions containing Ca^{2+}, such as the calcite-saturated solution, divalent cations would screen the negative charge, effectively delocalizing the charge on the surface or even reversing it. Hence, under our experimental conditions, we expect all of our SAMs to behave neutrally. For the uncharged surfaces, the COSMO-RS γ_{net} values are within the range of DFS values. (Table S5):

$$\text{COO(H)SAM (101−102 mJ/m}^2\text{)} < \text{NH}_2\text{SAM (110−115 mJ/m}^2\text{)} < \text{1/1 SAM (119−130mJ/m}^2\text{)}$$

Regardless of the charge on the surfaces, the COSMO-RS γ_{net} values follow the same trend as for γ_{net} extracted from the nucleation rate and DFS experiments. It is, however, noteworthy that the absolute values agree with γ_{net} from the DFS measurements.

3.4. Comparison of γ_{net} from Bulk, Molecular, and Computational Approaches. We find that the values for γ_{net} determined from DFS studies and COSMO-RS simulations are systematically higher than the values determined from the nucleation rate studies (Figure 7). The reason is that the nucleation rates are bulk measurements and, as such, include interparticle and solvent effects, which are negligible in molecular level studies such as DFS and absent in COMSO-RS computations. In addition, differences arise from comparing bulk system data with the DFS and COSMO-RS simulations, which were made using the {10.4} face of calcite, which is not necessarily the surface that nucleates on the SAMs (Figures S9−S11). However, this should not affect the relative relations among γ_{net} values obtained from different SAMs, only their absolute values. Hence, we used the DFS and COSMO results as a guide for determining trends and relations among γ_{net} values for the different surfaces, and not as an absolute measure of nucleation probability.

Regardless of the approach we used for determining the γ_{net} for calcite nucleation on a SAM, the trend is the same across the three different systems for the surfaces of:

$$\gamma_{net}\text{(B28SAM)} < \gamma_{net}\text{(COO(H)SAM)} < \gamma_{net}\text{(NH}_2\text{SAM)} < \gamma_{net}\text{(1/1SAM)}$$

The heterogeneous nucleation of calcite on any of those substrates is favorable only if $\gamma_{net} < (\gamma_{cl} = 103\text{ mJ/m}^2)$.[57,58] We crudely estimated the standard deviation for $\gamma_{cl} = 103 \pm 13$ mJ/m^2 by taking 103 mJ/m^2 as a mean value in comparison with the experimentally derived values of 97 mJ/m^2[57] and 120

https://dx.doi.org/10.1021/acs.cgd.0c00029
Cryst. Growth Des. 2020, 20, 3762−3771

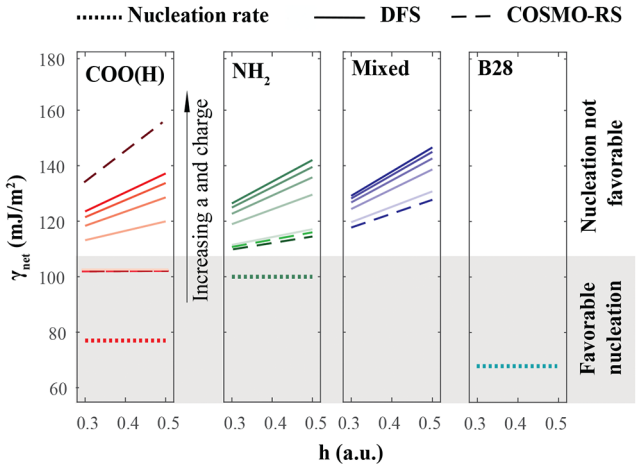

Figure 7. Interfacial free energy (γ_{net}) as a function of the shape factor (h) determined for the three model SAM substrates and the B28 surface using nucleation rate data (dotted line), DFS (full line), and COSMO calculations (dashed line). γ_{net} values for the DFS data were determined using a range of a values, shown as darker lines for higher values of a. For COSMO-RS calculations, the color of a line corresponds to the surface charge, with a light color denoting a neutral surface and a dark color denoting a charged surface. The gray field marks the range where $\gamma_{net} < (\gamma_{cl} = 103$ mJ/m^2). The uncertainties for the nucleation rate data and COSMO-RS calculations are given in Table S8 and uncertainties for the DFS data in Tables S3 and S4.

mJ/m^2.[58] This implies that the decrease in γ_{net} for calcite nucleation on a substrate in comparison to γ_{cl} in solution can be a driving force for calcite nucleation on carboxyl and amine SAMs but not on 1:1 SAM (Table 1), consistent with our observations (Figures S5–S7). The discrepancy between the nucleation rates for the B28 SAM and the 1:1 SAM highlights that the 1:1 SAM is not a good representation of the B28 SAM, likely because of the different distributions of carboxyl and amine functional groups on their surfaces. In general, our results imply that the preorganization of ionic functional groups by the peptoid backbone allows a higher density of potential productive nucleation sites, locally modifying γ_{net}. This illustrates the importance of controlling the positioning of multiple functional groups in precise orientation relative to one another. It also illustrates the importance of tunable materials such as peptoids, where atomic-level changes can be made to the structure to systematically improve their properties. That the B28 peptoid polymer substrate provides the lowest γ_{net} value of all surfaces investigated shows promising prospects of making targeted mineralization of nanosheets in a next step. It is interesting that while Jun et al.[10] obtained amorphous $CaCO_3$ on immobilized nanosheets at high and increasing saturation states, the nucleation observations and thermodynamic parameters derived here also hold promise for heterogeneously formed calcite on nanosheets using low-saturation conditions. A combination of the two approaches could open the possibility for some interesting designs of bulk mineralizing systems for mimicry of nacre properties. Fundamentally, the fact that two saturation regimes provide different results is not surprising but is something we should consider when testing how substrates can drive nucleation.

4. CONCLUSION

We used three approaches for obtaining the net interfacial free energy (γ_{net}) for calcite formation on B28 peptoid polymers and examined the potential for using peptoid nanosheets as scaffolds for biomimetic material applications from a bulk solution. We (a) studied nucleation rates on substrates comprising a monolayer of B28 peptoids and SAMs of carboxylic groups, amine groups, and a 1/1 mixture of the two as is represented on the B28 polymer, (b) applied dynamic force spectroscopy and obtained thermodynamic and kinetic parameters describing the interactions between calcite and carboxylic groups, amine groups, and a 1/1 substrate, and (c) used COSMO-RS for calculating the theoretical energies for binding between calcite and carboxylic, amine, and 1/1 SAMs. The obtained value for γ_{net} was the lowest for the B28 polymer (nucleation study only) and the values for the model surfaces were consistent among the three approaches: γ_{net} is lowest for carboxyl-terminated SAMs, followed by a higher value for the amine SAM, and the highest value for the 1:1 SAM. The relationship between the thermodynamic barrier of nucleation and the k.netic prefactor, derived from our nucleation studies, provides key insight into the solution conditions necessary for forming calcite on B28 nanosheet surfaces: at the studied saturation (σ), the nucleation rate (J_0) is orders of magnitude larger for calcite formation on carboxyl surfaces than for a monolayer of the B28 peptoid but at $\sigma < 3.3$ nucleation on the B28 substrate becomes favorable. Our results demonstrate that the B28 peptoid nanosheets can template $CaCO_3$ mineralization under low-saturation conditions and show potential for using B28-$CaCO_3$ as a nacre-mimicking material. The compositional tunability of peptoid nanosheets is a great property that could be used to further optimize the biomimicry in other systems.

■ ASSOCIATED CONTENT

Supporting Information

The Supporting Information is available free of charge at https://pubs.acs.org/doi/10.1021/acs.cgd.0c00029.

X-ray photoelectron spectroscopy of SAMs, PHREEQC modeling, scanning electron and optical microscopy images of nucleation rate experiments, dynamic force spectroscopy bond parameters, and COSMO-RS calculated parameters (PDF)

■ AUTHOR INFORMATION

Corresponding Author

Karina K. Sand − *Department of Geography & Earth Sciences, Aberystwyth University, Aberystwyth, United Kingdom;* orcid.org/0000-0002-0720-7229; Email: kks@sund.ku.dk

Authors

Anne R. Nielsen − *Nano-Science Center, Department of Chemistry, University of Copenhagen, Copenhagen, Denmark*

Stanislav Jelavić − *Nano-Science Center, Department of Chemistry, University of Copenhagen, Copenhagen, Denmark;* orcid.org/0000-0001-7854-3724

Daniel Murray − *Biological Nanostructures Facility, The Molecular Foundry, Lawrence Berkeley National Laboratory, Berkeley, California, United States*

Behzad Rad − *Biological Nanostructures Facility, The Molecular Foundry, Lawrence Berkeley National Laboratory, Berkeley, California, United States;* orcid.org/0000-0001-6531-9168

https://dx.doi.org/10.1021/acs.cgd.0c00029
Cryst. Growth Des. 2020, 20, 3762−3771

Martin P. Andersson − *Nano-Science Center, Department of Chemistry, University of Copenhagen, Copenhagen, Denmark;* orcid.org/0000-0002-4921-1461
Marcel Ceccato − *Nano-Science Center, Department of Chemistry, University of Copenhagen, Copenhagen, Denmark*
Andrew C. Mitchell − *Department of Geography & Earth Sciences, Aberystwyth University, Aberystwyth, United Kingdom*
Susan L. S. Stipp − *Nano-Science Center, Department of Chemistry, University of Copenhagen, Copenhagen, Denmark*
Ronald N. Zuckermann − *Biological Nanostructures Facility, The Molecular Foundry, Lawrence Berkeley National Laboratory, Berkeley, California, United States;* orcid.org/0000-0002-3055-8860

Complete contact information is available at: https://pubs.acs.org/10.1021/acs.cgd.0c00029

Notes

The authors declare no competing financial interest.

■ ACKNOWLEDGMENTS

Peptoid synthesis, method development for the B28 peptoids substrates preparation and design of the flow cell were carried out at the Molecular Foundry, Lawrence Berkeley National Laboratory, a Scientific User Facility supported by the U.S. Department of Energy, Office of Science and Office of Basic Energy Science under Contract No. DE-AC02-05CH11231 and User Proposal #3517. A.R.N. is grateful for additional funding granted by the Oticon Foundation, to support a research stay. A special thanks goes to Dr. Alessia Battigelli for synthesizing and purifying the B28 peptoid and to Michael Connolly and Rita Garcia for generous help at the Molecular Foundry. We thank the NanoGoeScience Group members for good scientific discussions. K.K.S. and A.C.M. are grateful for funding from the European Union's Horizon 2020 Research and Innovation Programme under Marie Skłodowska-Curie Grant Agreement No. 663830 and the Welsh Government and Higher Education Funding Council for Wales through the Sêr Cymru National Research Network for Low Carbon, Energy and Environment.

■ REFERENCES

(1) Weiner, S.; Addadi, L. Design Strategies in Mineralized Biological Materials. *J. Mater. Chem.* **1997**, *7*, 689−702.
(2) Nielsen, J. W.; Sand, K. K.; Pedersen, C. S.; Lakshtanov, L. Z.; Winther, J. R.; Willemoës, M.; Stipp, S. L. S. Polysaccharide Effects on Calcite Growth: The Influence of Composition and Branching. *Cryst. Growth Des.* **2012**, *12*, 4906−4910.
(3) Wegst, U. G. K.; Bai, H.; Saiz, E.; Tomsia, A. P.; Ritchie, R. O. Bioinspired Structural Materials. *Nat. Mater.* **2015**, *14*, 23−36.
(4) Sun, J.; Bhushan, B. Hierarchical Structure and Mechanical Properties of Nacre: A Review. *RSC Adv.* **2012**, *2*, 7617−7632.
(5) Bonderer, L. J.; Studart, A. R.; Gauckler, L. J. Bioinspired Design and Assembly of Platelet Reinforced Polymer Films. *Science* **2008**, *319*, 1069−1073.
(6) Farhadi-Khouzani, M.; Schütz, C.; Durak, G. M.; Fornell, J.; Sort, J.; Salazar-Alvarez, G.; Bergström, L.; Gebauer, D. A CaCO3/Nanocellulose-Based Bioinspired Nacre-like Material. *J. Mater. Chem. A* **2017**, *5*, 16128−16133.
(7) Fritz, M.; Belcher, A. M.; Radmacher, M.; Walters, D. A.; Hansma, P. K.; Stucky, G. D.; Morse, D. E.; Mann, S. Flat Pearls from Biofabrication of Organized Composites on Inorganic Substrates. *Nature* **1994**, *371*, 49−51.
(8) Wei, Y.-Z.; Wang, G.-S.; Wu, Y.; Yue, Y.-H.; Wu, J.-T.; Lu, C.; Guo, L. Bioinspired Design and Assembly of Platelet Reinforced Polymer Films with Enhanced Absorption Properties. *J. Mater. Chem. A* **2014**, *2*, 5516−5524.
(9) Finnemore, A.; Cunha, P.; Shean, T.; Vignolini, S.; Guldin, S.; Oyen, M.; Steiner, U. Biomimetic Layer-by-Layer Assembly of Artificial Nacre. *Nat. Commun.* **2012**, *3*, 966.
(10) Jun, J. M. V.; Altoe, M. V. P.; Aloni, S.; Zuckermann, R. N. Peptoid Nanosheets as Soluble, Two-Dimensional Templates for Calcium Carbonate Mineralization. *Chem. Commun.* **2015**, *51*, 10218−10221.
(11) Zuckermann, R. N.; Kerr, J. M.; Kent, S. B. H.; Moos, W. H. Efficient Method for the Preparation of Peptoids [Oligo(N-Substituted Glycines)] by Submonomer Solid-Phase Synthesis. *J. Am. Chem. Soc.* **1992**, *114*, 10646−10647.
(12) Sun, J.; Zuckermann, R. N. Peptoid Polymers: A Highly Designable Bioinspired Material. *ACS Nano* **2013**, *7*, 4715−4732.
(13) Mannige, R. V.; Haxton, T. K.; Proulx, C.; Robertson, E. J.; Battigelli, A.; Butterfoss, G. L.; Zuckermann, R. N.; Whitelam, S. Peptoid Nanosheets Exhibit a New Secondary-Structure Motif. *Nature* **2015**, *526*, 415−420.
(14) Robertson, E. J.; Olivier, G. K.; Qian, M.; Proulx, C.; Zuckermann, R. N.; Richmond, G. L. Assembly and Molecular Order of Two-Dimensional Peptoid Nanosheets through the Oil−Water Interface. *Proc. Natl. Acad. Sci. U. S. A.* **2014**, *111*, 13284−13289.
(15) Sanii, B.; Kudirka, R.; Cho, A.; Venkateswaran, N.; Olivier, G. K.; Olson, A. M.; Tran, H.; Harada, R. M.; Tan, L.; Zuckermann, R. N. Shaken, Not Stirred: Collapsing a Peptoid Monolayer to Produce Free-Floating, Stable Nanosheets. *J. Am. Chem. Soc.* **2011**, *133*, 20808−20815.
(16) Kudirka, R.; Tran, H.; Sanii, B.; Nam, K. T.; Choi, P. H.; Venkateswaran, N.; Chen, R.; Whitelam, S.; Zuckermann, R. N. Folding of a Single-Chain, Information-Rich Polypeptoid Sequence into a Highly Ordered Nanosheet. *Biopolymers* **2011**, *96*, 586−595.
(17) Nam, K. T.; Shelby, S. A.; Choi, P. H.; Marciel, A. B.; Chen, R.; Tan, L.; Chu, T. K.; Mesch, R. A.; Lee, B.-C.; Connolly, M. D.; Kisielowski, C.; Zuckermann, R. N. Free-Floating Ultrathin Two-Dimensional Crystals from Sequence-Specific Peptoid Polymers. *Nat. Mater.* **2010**, *9*, 454−460.
(18) Chen, C.-L.; Qi, J.; Tao, J.; Zuckermann, R. N.; DeYoreo, J. J. Tuning Calcite Morphology and Growth Acceleration by a Rational Design of Highly Stable Protein-Mimetics. *Sci. Rep.* **2015**, *4*, 6266.
(19) Smeets, P. J. M.; Cho, K. R.; Sommerdijk, N. A. J. M.; Yoreo, J. J. D. A Mesocrystal-Like Morphology Formed by Classical Polymer-Mediated Crystal Growth. *Adv. Funct. Mater.* **2017**, *27*, 1701658.
(20) Smeets, P. J. M.; Cho, K. R.; Kempen, R. G. E.; Sommerdijk, N. A. J. M.; De Yoreo, J. J. Calcium Carbonate Nucleation Driven by Ion Binding in a Biomimetic Matrix Revealed by *in Situ* Electron Microscopy. *Nat. Mater.* **2015**, *14*, 394−399.
(21) Nielsen, A. E. *Kinetics of Precipitation*; Pergamon Press: Oxford and New York, 1964.
(22) De Yoreo, J. J.; Waychunas, G. A.; Jun, Y.-S.; Fernandez-Martinez, A. In Situ Investigations of Carbonate Nucleation on Mineral and Organic Surfaces. *Rev. Mineral. Geochem.* **2013**, *77*, 229−257.
(23) Hu, Q.; Nielsen, M. H.; Freeman, C. L.; Hamm, L. M.; Tao, J.; Lee, J. R. I.; Han, T. Y. J.; Becker, U.; Harding, J. H.; Dove, P. M.; De Yoreo, J. J. The Thermodynamics of Calcite Nucleation at Organic Interfaces: Classical vs. Non-Classical Pathways. *Faraday Discuss.* **2012**, *159*, 509−523.
(24) Hamm, L. M.; Giuffre, A. J.; Han, N.; Tao, J.; Wang, D.; Yoreo, J. J. D.; Dove, P. M. Reconciling Disparate Views of Template-Directed Nucleation through Measurement of Calcite Nucleation Kinetics and Binding Energies. *Proc. Natl. Acad. Sci. U. S. A.* **2014**, *111*, 1304−1309.
(25) Giuffre, A. J.; Hamm, L. M.; Han, N.; Yoreo, J. J. D.; Dove, P. M. Polysaccharide Chemistry Regulates Kinetics of Calcite Nucleation through Competition of Interfacial Energies. *Proc. Natl. Acad. Sci. U. S. A.* **2013**, *110*, 9261−9266.
(26) Ulman, A. Formation and Structure of Self-Assembled Monolayers. *Chem. Rev.* **1996**, *96*, 1533−1554.

(27) Lewis, P. A.; Donhauser, Z. J.; Mantooth, B. A.; Smith, R. K.; Bumm, L. A.; Kelly, K. F.; Weiss, P. S. Control and Placement of Molecules via Self-Assembly. *Nanotechnology* **2001**, *12*, 231−237.
(28) Nielsen, M. H.; Lee, J. R. I.; De Yoreo, J. J. Preparation of Organothiol Self-Assembled Monolayers for Use in Templated Crystallization. *Methods Enzymol.* **2013**, *532*, 209−224.
(29) Chuang, W.-H.; Lin, J.-C. Surface Characterization and Platelet Adhesion Studies for the Mixed Self-Assembled Monolayers with Amine and Carboxylic Acid Terminated Functionalities. *J. Biomed. Mater. Res., Part A* **2007**, *82A*, 820−830.
(30) Nielsen, M. H.; Lee, J. R. I.; Hu, Q.; Han, T. Y.-J.; Yoreo, J. J. D. Structural Evolution, Formation Pathways and Energetic Controls during Template-Directed Nucleation of CaCO3. *Faraday Discuss.* **2012**, *159*, 105−121.
(31) Parkhurst, D. L. *User's Guide to PHREEQC, a Computer Program for Speciation, Reaction-Path, Advective-Transport, and Inverse Geochemical Calculations; Water-Resources Investigations Report*; U.S. Geological Survey, Earth Science Information Center: 1995; Open-File Reports Section, USGS Numbered Series 95-4227.
(32) Plummer, N.; Busenberg, E. The Solubilities of Calcite, Aragonite and Vaterite in CO_2-H_2O Solutions between 0 and 90°C, and an Evaluation of the Aqueous Model for the System CaCO3-CO2-H2O. *Geochim. Cosmochim. Acta* **1982**, *46*, 1011.
(33) Burnham, N. A.; Chen, X.; Hodges, C. S.; Matei, G. A.; Thoreson, E. J.; Roberts, C. J.; Davies, M. C.; Tendler, S. J. B. Comparison of Calibration Methods for Atomic-Force Microscopy Cantilevers. *Nanotechnology* **2003**, *14*, 1−6.
(34) Friddle, R. W.; Noy, A.; De Yoreo, J. J. Interpreting the Widespread Nonlinear Force Spectra of Intermolecular Bonds. *Proc. Natl. Acad. Sci. U. S. A.* **2012**, *109*, 13573−13578.
(35) Klamt, A.; Eckert, F.; Arlt, W. COSMO-RS: An Alternative to Simulation for Calculating Thermodynamic Properties of Liquid Mixtures. *Annu. Rev. Chem. Biomol. Eng.* **2010**, *1*, 101−122.
(36) Ahlrichs, R.; Bär, M.; Häser, M.; Horn, H.; Kölmel, C. Electronic Structure Calculations on Workstation Computers: The Program System Turbomole. *Chem. Phys. Lett.* **1989**, *162*, 165−169.
(37) Perdew, J. P. Density-Functional Approximation for the Correlation Energy of the Inhomogeneous Electron Gas. *Phys. Rev. B: Condens. Matter Mater. Phys.* **1986**, *33*, 8822−8824.
(38) Becke, A. D. Density-Functional Exchange-Energy Approximation with Correct Asymptotic Behavior. *Phys. Rev. A: At., Mol., Opt. Phys.* **1988**, *38*, 3098−3100.
(39) Weigend, F.; Ahlrichs, R. Balanced Basis Sets of Split Valence, Triple Zeta Valence and Quadruple Zeta Valence Quality for H to Rn: Design and Assessment of Accuracy. *Phys. Chem. Chem. Phys.* **2005**, *7*, 3297−3305.
(40) Klamt, A.; Schüürmann, G. COSMO: A New Approach to Dielectric Screening in Solvents with Explicit Expressions for the Screening Energy and Its Gradient. *J. Chem. Soc., Perkin Trans. 2* **1993**, *0*, 799−805.
(41) Andersson, M. P.; Olsson, M. H. M.; Stipp, S. L. S. Predicting the PKa and Stability of Organic Acids and Bases at an Oil−Water Interface. *Langmuir* **2014**, *30*, 6437−6445.
(42) Andersson, M. P.; Hassenkam, T.; Matthiesen, J.; Okhrimenko, D. V.; Dobberschütz, S.; Stipp, S. L. S. First-Principles Prediction of Surface Wetting; *Unpublished work*.
(43) Andersson, M. P.; Bennetzen, M. V.; Klamt, A.; Stipp, S. L. S. First-Principles Prediction of Liquid/Liquid Interfacial Tension. *J. Chem. Theory Comput.* **2014**, *10*, 3401−3408.
(44) Andersson, M. P.; Eckert, F.; Reinisch, J.; Klamt, A. Prediction of Aliphatic and Aromatic Oil-Water Interfacial Tension at Temperatures > 100 °C Using COSMO-RS. *Fluid Phase Equilib.* **2018**, *476*, 25−29.
(45) Murray, D. J.; Kim, J. H.; Grzincic, E. M.; Kim, S. C.; Abate, A. R.; Zuckermann, R. N. Uniform, Large-Area, Highly Ordered Peptoid Monolayer and Bilayer Films for Sensing Applications. *Langmuir* **2019**, *35*, 13671−13680.
(46) Soula, H.; Caré, B.; Beslon, G.; Berry, H. Anomalous versus Slowed-Down Brownian Diffusion in the Ligand-Binding Equilibrium. *Biophys. J.* **2013**, *105*, 2064−2073.
(47) De Yoreo, J. J.; Vekilov, P. G. Principles of Crystal Nucleation and Growth. In *Biomineralization*; Mineralogical Society of America: 2003; Vol. *54*, pp 57−93.
(48) Olivier, G. K.; Cho, A.; Sanii, B.; Connolly, M. D.; Tran, H.; Zuckermann, R. N. Antibody-Mimetic Peptoid Nanosheets for Molecular Recognition. *ACS Nano* **2013**, *7*, 9276−9286.
(49) Han, Y.-J.; Aizenberg, J. Face-Selective Nucleation of Calcite on Self-Assembled Monolayers of Alkanethiols: Effect of the Parity of the Alkyl Chain. *Angew. Chem.* **2003**, *115*, 3796−3798.
(50) Aizenberg, J.; Black, A. J.; Whitesides, G. M. Oriented Growth of Calcite Controlled by Self-Assembled Monolayers of Functionalized Alkanethiols Supported on Gold and Silver. *J. Am. Chem. Soc.* **1999**, *121*, 4500−4509.
(51) Somasundaran, P.; Agar, G. E. The Zero Point of Charge of Calcite. *J. Colloid Interface Sci.* **1967**, *24*, 433−440.
(52) Söhnel, O. Electrolyte Crystal-Aqueous Solution Interfacial Tensions from Crystallization Data. *J. Cryst. Growth* **1982**, *57*, 101−108.
(53) Söhnel, O. Estimation of Electrolyte-Crystal-Aqueous-Solution Interfacial Tension. *J. Cryst. Growth* **1983**, *63*, 174−176.
(54) Travaille, A. M.; Steijven, E. G. A.; Meekes, H.; van Kempen, H. Thermodynamics of Epitaxial Calcite Nucleation on Self-Assembled Monolayers. *J. Phys. Chem. B* **2005**, *109*, 5618−5626.
(55) Duffy, D. M.; Harding, J. H. Simulation of Organic Monolayers as Templates for the Nucleation of Calcite Crystals. *Langmuir* **2004**, *20*, 7630−7636.
(56) Lide, D. R. *CRC Handbook of Chemistry and Physics*, 72nd ed.; CRC Press: 1991.
(57) Söhnel, O.; Mullin, J. W. Precipitation of Calcium Carbonate. *J. Cryst. Growth* **1982**, *60*, 239−250.
(58) Söhnel, O.; Mullin, J. W. A Method for the Determination of Precipitation Induction Periods. *J. Cryst. Growth* **1978**, *44*, 377−382.

https://dx.doi.org/10.1021/acs.cgd.0c00029
Cryst. Growth Des. 2020, 20, 3762−3771